ORIGINAL PAPER

Effects of Artisanal Biochar Applied to Rice Cultivation in Fragile Sandy Planosol at Rio de Janeiro (Brazil)

Danielle França de Oliveira Torchia[1] · Tadeu Augusto van Tol de Castro[1] · Orlando Carlos Huertas Tavares[1] ·
Camila Costa Barros Souza[2] · Hellen Fernanda Oliveira da Silva[1] · Octávio Vioratti Telles de Moura[1] ·
Kimberly Christina Marques da Silva[1] · Franciele de Souza Rocha[1] · Everaldo Zonta[3] · Andrés Calderín García[1]

Abstract

This study aimed to investigate the influence of chemical and structural characteristics of biochar on the development of rice plants grown in fragile sandy soil. An experiment was carried out in pots with the application of four doses (0 ton ha^{-1}; 10 ton ha^{-1}; 20 ton ha^{-1}; 30 ton ha^{-1}) of eucalyptus biochar from four artisanal sources (B1, B2, B3, and B4). Fresh root mass increased by 0.56% with the application of biochar B4 and decreased with the application of biochars B1, B2, and B3 (23.3%; 18.3%; 19.9%). The fresh mass of sheath and leaves decreased by an average of 23.6% and 27%, respectively, with the application of all biochars. Root dry mass increased by 7.8% with the application of biochar B4 and decreased with the application of B1, B2, and B3. The sheath dry mass and leaf dry mass decreased by an average of 20.2% and 25.1%, respectively, with the application of all biochars. The nutrient content, specifically P, K, and N, increased with the application of B1, B2, and B3. The application of biochar B4 (30 ton ha^{-1}) lessened the damage to the photosynthetic apparatus and promoted physiological recovery. The beneficial effect of biochar B4 occurred at a dose of 30 ton ha^{-1} in the reaction centers, increasing photochemical efficiency in photosystem II. Root development was stimulated by the application of biochar B4, increasing root area by 55% (10 ton ha^{-1}) and 56% (20 ton ha^{-1} and 30 ton ha^{-1}). The total length increased by 48% with the application of biochar B4 and by 27% with biochar B2 (30 ton ha^{-1}). The length of thick roots and the total root volume were less affected by the treatments, with increases of approximately 11% and 7%, respectively. Although most treatments did not result in higher biomass production compared to the control, there was a notable increase in nutrient content in the aboveground portion, particularly with the application of biochar B2. Furthermore, improvements in photosynthetic parameters and root morphology were observed, particularly when biochar B4 was applied. Overall, the findings of this study indicate that biochars B2 and B4, at rates of 20 and 30 ton ha^{-1}, respectively, hold promise for enhancing cultivation in vulnerable Planosols in the Rio de Janeiro region of Brazil. However, to fully understand the effects on soil properties in different crops and the economic implications of implementing biochar in agriculture, further long-term and large-scale research is necessary.

Keywords Biochar · Fragile Planosol · Photosynthetic quantum efficiency · Root growth

Highlights
- The artisanal biochars studied exhibit different structural characteristics, with B1 and B4 being more aromatic, and B2 and B3 being more aliphatic.
- The application of artisanal biochar B4 results in up to 24% higher biomass production in rice plants compared to the application of biochars B1, B2, and B3.
- Biochar B2 leads to a 50% increase in phosphorus accumulation in the aboveground part of rice plants.
- The application of biochar B4 promotes greater increases in root volume, area, length, and the number of tips and forks.

Extended author information available on the last page of the article

1 Introduction

The predominant agriculture in the state of Rio de Janeiro, Brazil (RJ), is conducted on poor soils with low carbon fixation capacity, low organic matter content, low fertility, and nutrient availability (especially phosphorus), prone to erosion and abiotic stresses, classified as Planosols. The agricultural model is mainly developed by small-scale family farming and produces the majority of the food consumed in different municipalities today. Small farmers struggle with reduced incomes and limited availability of inputs that improve the chemical, physical, biological, and natural

fertility conditions of their soils. In this context, the currently available alternatives are limited to controversial no-till practices with long-term returns and the use of labile compounds with relatively high mineralization rates (Demetrio et al. 2020).

It is therefore urgent to propose more precise and targeted solutions for agriculture in the state of Rio de Janeiro. Under these conditions, the exogenous application of stabilized carbon, such as biochar, can contribute to the accumulation of organic matter, as these carbons have slow decomposition rates and longer residence time in the soil. Pyrolyzed carbon has mineralization rates 10 to 100 times lower than those of the biomass of origin and, therefore, can persist in the soil for decades, depending on soil type, climate, and environmental conditions (Paustian et al. 2016; Lehmann and Joseph 2015). Moreover, biochar is easily produced by small producers, is economically viable, and can be made from a wide range of biomass types. In recent years, biochar has become one of the most studied materials to improve the physical, chemical, and biological properties of sandy soils (Das et al. 2023; Dokoohaki et al. 2017; Li et al. 2021). Application of biochar to acidic and sandy soil increased soil porosity, aggregate stability, weight-average diameter, water-holding capacity, and soil moisture content (Das and Ghosh 2022a). Biochar application in soil has great potential to increase fertility, nutrient content, nutrient use efficiency, water holding capacity, and consequently, productivity related to soil properties and plant biomass growth (Das and Ghosh 2022a; Regmi et al. 2022; Semida et al. 2019). The application of biochar together with organic fertilizer significantly increased the content of protein, ash, tannin, C, N, P, K, Zn, Fe, Cu, Mn, and B in maize-black gram, cultivated in an acidic hilly soil (Das et al. 2022). Furthermore, biochar applied with organic fertilizer improves the soil's carbon sequestration capacity, being a promising strategy for regeneration of sandy soils (Das et al. 2023).

Many studies worldwide have evaluated the benefits of biochar application for soil and plant development (Das et al. 2021; Das and Ghosh 2022b), but few or none have been specifically directed towards Planosols in the state of RJ. Therefore, the present investigation was designed to study the effect of biochar on nutrient-deficient sandy Planosols for rice cultivation. For this purpose, four artisanal biochars were characterized using chemical and structural techniques. Subsequently, they were applied in a pot experiment with 2 kg of soil, cultivating *Oryza sativa* L. (cv. Nipponbare) rice in Planosols, at application rates of 10 ton ha^{-1}, 20 ton ha^{-1}, and 30 ton ha^{-1}. The parameters of plant growth, biomass production, nutrients accumulated in the aboveground part of the plant, transient fluorescence emission of chlorophyll a, and root morphology were evaluated. The investigation also aimed to examine the influence of different structures of artisanal biochars on plant growth parameters.

The biochars investigated in this study contributed to enhance rice cultivation. Although most treatments did not result in higher biomass production than the control, there was a notable increase in nutrient content in the aboveground portion, particularly with the application of biochar B2. Furthermore, improvements in photosynthetic parameters and root morphology were observed, particularly when biochar B4 was applied. Overall, the findings of this study indicate that biochars B2 and B4, at rates of 20 and 30 ton ha^{-1}, respectively, hold promise for enhancing cultivation in vulnerable Planosols in the Rio de Janeiro region of Brazil. However, to fully understand the effects on soil properties in different crops and the economic implications of implementing biochar in agriculture, further long-term and large-scale research is necessary.

2 Materials and Methods

2.1 Sources of the Different Biochars Used in This Study

The biochar used in this study was collected from charcoal production carried out in charcoal kilns by local producers in the Baixada Fluminense region in the state of Rio de Janeiro, Brazil. The coal was obtained by carbonization of biomass from wood residue. The producers indicated that the production conditions may correspond to a temperature of 270 to 380 °C and a time of 24 h. Subsequently, the biochars were characterized and applied to the soil in a rice plant development test, as per the flowchart in Fig. S1.

2.2 ATR-FTIR Structural Characterization of Artisanal Biochar

Attenuated total reflection (ATR)-Fourier transform infrared spectroscopy (FTIR) spectra were obtained by recording in the wavenumber region of 400.00 to 4000.00 cm^{-1} with a spectral resolution of 4 cm^{-1}, collecting 32 scans in each measurement. For this purpose, a VERTEX 70/70v FTIR spectrometer (Bruker Corporation, Germany) was coupled to a diamond-platinum ATR device consisting of a diamond disk that functions as an internal reflection element. The materials were placed on the ATR crystal to record the spectrum. The air spectrum was collected before each analysis as background. Spectral collection was performed using OPUS-Bruker software (García et al. 2016).

2.3 CP-MAS ^{13}C NMR Structural Characterization of Artisanal Biochar

Cross polarization/magic angle spinning (CP/MAS) ^{13}C nuclear magnetic resonance (NMR) analysis was performed at the Analytical Center of PPGQ/UFRRJ with a 400 MHz

Bruker AVANCE II NMR instrument equipped with a 4-mm narrow MAS probe and operating at a ^{13}C resonance sequence from 100 to 163 MHz. The samples were placed in a zirconium dioxide (ZrO_2) rotor (sample holder) with Kel-F caps at a rotation frequency of 8 ± 1 kHz. The spectra were selected by collecting 2283 data points for a fixed number of scans in a capture time of 34 ms with a recycling delay of 5 s. The contact time for the 1 H ramp sequence was 2 ms. Spectral collection and elaboration were performed using Bruker Topspin 2.1 software. The free induction decays (FIDs) were transformed by applying a zero padding of 4 k followed by an exponential function fit (line extension) of 70 Hz. The spectra were analyzed using the software ACD/Labs v.12.01 (Freeware Academic Edition). To calculate the relative amount of carbon types, the spectra were divided into chemical shifts, and the areas were determined after integration of each region and expressed as the percentage of the total area. The regions were designated as follows: alkyl C (C_{alkyl}-H,R) 0–45 ppm; methoxyl and N–C (C_{alkyl}-O,N) 45–60 ppm; O–C (C_{alkyl}-O) 60–90 ppm; alkyl di-O–C (anomeric) (C_{alkyl}-*di*-O) 90–110 ppm; aromatic C ($C_{aromatic}$-H,R) 110–145 ppm; O,N-aromatic C ($C_{aromatic}$-O,N) 145–160 ppm; carboxyl C (C_{COO}-H,R) 160–190 ppm; and carbonyl C ($C_{C=O}$) 190–220 ppm. The aromaticity, aliphaticity, and hydrophobic index was calculated as follows (Mazzei et al. 2022):

$$\text{Aromaticity} = [(110 - 145\text{ppm}) + (145 - 160\text{ppm})]$$

$$\text{Aliphaticity} = [(0 - 45\text{ppm}) + (45 - 60\text{ppm}) + (60 - 90\text{ppm}) \\ + (90 - 110\text{ppm}) + (160 - 190\text{ppm}) + (190 - 220\text{ppm})]$$

$$\text{Hydrophobic index} = [(0 - 45\text{ppm}) + (45 - 60\text{ppm}) \\ + (110 - 145\text{ppm}) + (145 - 160\text{ppm})] \\ /[(60 - 90\text{ppm}) + (90 - 110\text{ppm}) \\ + (160 - 190\text{ppm}) + (190 - 220\text{ppm})]$$

Chemometric analyses (principal component analysis (PCA) and multivariate curve resolution (MCR) of the ^{13}C NMR CP/MAS and ATR-FTIR spectra were performed using the software Unscrambler X 10.3 (Camo Software AS. Inc. Oslo, Norway).

2.4 Growth Conditions, Plant Material, Experimental Design, and Statistical Analysis

The experiment was conducted with *Oryza sativa* L. (cv. Nipponbare) in a greenhouse. The rice seeds were previously disinfected with sodium hypochlorite (2%) for 10 min and washed with distilled water. Then, they were sown in pots containing 2 kg of soil at a depth of 3 cm. The chemical analysis of the soil used in the experiment is shown in Table S1. Nutritional supplementation was performed at 21 and 26 days after sowing (DAS) to meet the phosphorus requirements due to deficiency expressed by visual symptoms, applying 31 ppm of phosphorus from two sources: 2/3 monobasic potassium phosphate (KH_2PO_4) and 1/3 anhydrous dibasic potassium phosphate (K_2HPO_4). The application forms and sources were selected according to the need for rapid absorption and assimilation of this macronutrient by plants. The harvest was performed at 32 DAS.

Four artisanal biochars (B1, B2, B3, and B4) and three doses (10 ton ha^{-1}, 20 ton ha^{-1}, and 30 ton ha^{-1}) were studied. The experimental design adopted was a completely randomized factorial design with an additional treatment and seven replicates $((4 \times 3 + 1) \times 7)$. Statistical analyses were performed using R statistical software. The data were subjected to two-way analysis of variance (ANOVA) with interaction. When a significant difference was indicated by the ANOVA *F* test ($p < 0.5$), means tests were performed using Tukey's test ($p < 0.05$). The data were ordered by principal component analysis. Graphs were prepared using R statistical software, Sigmaplot 12.0.

2.4.1 Macro and Micronutrients in Plant Tissues and Biochar Samples

For the quantification of macro- and micronutrients, the samples were first pretreated by acid digestion, adapted from the EPA 3050 method. A sample mass of 0.25 g was weighed and placed in a digestion tube. A volume of 5 ml of nitric acid (HNO$_3$ PA) was added to each tube and placed in the digester block in a fume hood for 15 min at 95 °C. Subsequently, another 10 ml of nitric acid was added to the tubes, which were kept in the digester block for another 2 h. The samples were removed from the digester block, and 8 ml of hydrogen peroxide (H_2O_2) was added. The volume of the sample was brought to 50 ml with distilled water, and the sample was then filtered. Nutrient quantification was performed with an atomic absorption spectroscope (VARIAN 55B), K^+ content was determined with a flame photometer (DIGIMED DM-62), and P content was determined by the colorimetric method (Malavolta et al. 1997).

2.4.2 Evaluation of the Transient Fluorescence Parameters of Chlorophyll a and JIP Test Analysis

The leaves were adapted in the dark for at least 30 min before measurements. Chlorophyll *a* fluorescence parameters were measured using the Handy Plant Efficiency Analyzer (Plant Efficiency Analyzer; Hansatech, UK). The measurement light source was three light-emitting diodes providing red light with a wavelength of 650 nm and a light intensity of

3000 μmol m^{-2} s^{-1}, and data were recorded for 1 s. The measurements were performed at 7:00 am. Data were collected at two time points, 26 DAS and 32 DAS. An OJIP curve was plotted to normalize the fluorescence data to the relative variable fluorescence data using the following equation:

Vt = (Ft − Fo)/(FM − Fo), where Vt is the relative variable fluorescence at time *t*, Fo is the initial fluorescence, Ft is the fluorescence at time *t*, and FM is the maximum fluorescence.

The JIP test parameters (transient fluorescence stages O, J, I, and P) were calculated according to the JIP test algorithm described by (Strasser et al. 2004).

2.4.3 Measurements of Root System Morphology and Biomass Accumulation

The root systems of the rice plants were evenly distributed in a layer of water in a transparent acrylic tray (30 cm × 20 cm), and the plants were scanned at 600 dpi with an Epson Expression 10000XL scanner with additional lighting (transparency unit (TPU)) (Tavares et al. 2021). The use of an additional light source above the scanner promoted a higher scanning resolution, improving image quality and analysis results. The images of the roots were converted to an eight-bit grayscale format. These images were individually processed and analyzed, and a total of five root parameters were quantified: root length (m plant^{-1}), root surface area (m^2 plant^{-1}), mean root diameter (mm root^{-1} plant^{-1}), volume (m^3 plant^{-1}), root branches (n° plant^{-1}), and root tips (n° plant^{-1}).

To evaluate the fresh weight of the plants, the leaves, sheaths, and root system of each plant were separated and weighed on a precision digital scale. Next, the samples were placed in paper envelopes and transferred to a drying oven, where they were kept for 72 h at 60 °C. After this period, the dry mass of the roots and shoots was weighed on a precision digital scale.

3 Results

3.1 Macro and Micronutrients in Artisanal Biochar

The total levels of N, C, H, and O in the biochars are shown in Table 1. The biochars have high C contents, all above 60%, and are considered class 1, according to the standards proposed by the International Biochar Initiative. Low N, O, and H concentrations were observed. Biochar (B3) had higher N (1%) and O (29.2%) content but lower H content (3.2%). The O:C ratio, which indicates the polarity and abundance of surface functional groups containing O in biochar, was highest in B3 (0.44) and lowest in B1 (0.23). Conversely, the H:C ratio, which indicates stability

and the presence of aromatic fragments, had a higher value in B2 and B4 (0.06). Regarding macro and micronutrients, the high values of P in biochars B3 and B4 (273.57 g kg^{-1} and 274.57 g kg^{-1}) and the low levels of Ca and Mg in B1 (0.70 g kg^{-1} and 10.58 g kg^{-1}) stand out. Photosynthetic fixation of C in plants through N or P accumulation is expressed by C:N and C:P ratios. Biochar (B4) showed the highest value in the C:N ratio (452.8). The C:P ratio was higher in B2 (3.97), and the N:P value was higher in B2, which indicate P limitation.

Through the PCA shown in Fig. S2 (85% of the total explained variance), it is possible to observe the compositional differences among the biochars. PC-1 (68% of the explained variance) groups biochar B3 and B4 with negative values, confirming the higher contents of P in B3 and B4 than in B1 and B2. Also grouped with negative values, B3 and B4 showed a greater presence of all quantified nutrients, Fe, Mg, Ca, K, Cu, and Mn. Biochars B3 and B4 differ in their chemical properties. PC-2 (17% of the explained variance) showed that B3 has a higher O:C ratio and O content, indicating a more hydrophobic material with a slightly more functionalized structure. The PCA confirmed that in nutritional terms, B1 and B2 are more deficient in nutrients than B3 and B4.

3.2 ATR-FTIR Structural Characterization of Artisanal Biochar

The FTIR spectra show the functional groups present in the different biochars (Fig. S3a). The studied biochars have similar spectra; however, certain bands stand out in some materials due to their intensity. In biochar, the bands in the regions of ~3371.18 cm^{-1} and ~3199.53 cm^{-1} indicate -OH and -NH groups belonging to amides and carboxyls, and these bands are more evident in B4 than in B2. The band in the ~2921.82 cm^{-1} region corresponding to -CH groups of -CH$_3$ fragments is again more evident in the spectrum of B4 than that of B2. The band in the range 2960–2850 cm^{-1} corresponds to aliphatic groups, which are an indication of cellulose, hemicellulose, and lignin in the precursor (Antonangelo et al. 2019; Reza et al. 2020). The band in the ~1593.02 cm^{-1} region indicates C=C groups, and this band is more pronounced in B4. The ~1216.94 cm^{-1} region is attributed to -CN in alkyl-amine structures and has greater intensity in B4. The band in the region of ~781.08 cm^{-1} refers to CH groups belonging to aromatic carbons and benzene chains (Lopes and Fascio 2004).

Chemometric analyses revealed detailed information about the differences in the FTIR spectra. The PCA scores and loadings for the FTIR data (96% of the total explained variance) are shown in Fig. S3b and S3c, respectively. The PCA scores confirmed structural similarity between biochars B3 and B4, grouped at positive values of PC-1 (90% of explained variance) and similarity between B2 and B1, grouped at negative

values of PC-1. The loadings of PC-1 showed that B3 and B4 are similar due to the predominance of -OH, -NH, -COOH, and -COO$^-$ functional groups, while B1 and B2 are structurally related due to the presence of C=C structures. The PC2 loadings showed differences between B2 and B1 with the predominance of C=C in the former and CH in the latter.

3.3 ^{13}C NMR CP/MAS Structural Characterization of Artisanal Biochar

The ^{13}C NMR spectra showed a similar spectral and structural pattern among the biochars (Fig. S4a). The peaks in the aliphatic region (0–110 ppm) corresponding to C_{alkyl}-O, C_{alkyl}-di-O and C_{alkyl} groups contributed negligibly to the composition of the biochars. C_{alkyl} and C_{alkyl}-O correspond to polysaccharides such as cellulose and hemicellulose and were less expressed in B2 (Bonanomi et al. 2018; Kogel-Knabner 2002). The regions from 110–140 ppm and 140–160 ppm showed the predominance of aromatic carbon fragments, related to the condensation of aromatic structures produced from the carbonization process (García et al. 2019).

Figure S4b shows the PCA results of the ^{13}C NMR data (94% of the total explained variance). The scores showed differences in biochar composition, in which B1 and B2 were clustered at positive values of PC-1 (61% of the total explained variance), while B3 and B4 were clustered at negative values. Again, the structural differentiation captured by NMR was consistent with the results obtained by ATR-FTIR and by elemental composition analysis. Figure S4c shows the MCR curve, which indicates patterns of greater and

lesser hydrophobicity as predominant domains in the biochar structures; no pattern of hydrophilicity was observed.

The relative quantification of the types of carbon in the different biochars is presented in Fig. S4d. In general, B1 showed the highest amount of C_{alkyl}-di-O structures. Biochar (B2) predominantly contains functionalized aromatic carbons of the form C_{arom}-O,N. B3 has a predominance of aliphatic and carbonyl structures of the types C_{alkyl}-H,R and C=O, respectively. B4 is structurally predominant in C_{arom}-H,R. Such structural characteristics promote greater aromaticity in B1 and B4 and, consequently, lower aliphaticity. B1 showed the highest hydrophobicity, followed by B4.

3.4 Effects of Biochar Application on Rice Plant Biomass

The effects of the application of different biochars on the production of fresh and dry mass of roots, sheaths, and leaves are shown in Fig. 1. The fresh root mass (Fig. 1a) was more stimulated with the application of B4 at all doses (4.22 g pot^{-1}), with increases of 24%, 20%, and 18% compared with the responses to B1, B3, and B2, respectively. Dry mass was also more strongly stimulated by the application of B4 (0.38 g pot^{-1}), with increases of 13% and 18% compared to B2 and B3 and 21% compared to B1.

Sheath biomass slightly decreased with the biochar treatments. Compared to the control, the application of treatments did not stimulate the production of fresh sheath mass (Fig. 1b); however, it is noteworthy that the application of B4 at all doses promoted the response most similar to the control treatment. The sheath fresh mass was 17% higher in B4 (1.82 g pot^{-1}) compared to B1 and B3 (1.51 g pot^{-1})

Table 1 Macro and micronutrients in artisanal biochars

	B1	B2	B3	B4
N (%)	0.6 ± 0.02	0.7 ± 0.21	1.0 ± 0.32	0.2 ± 0.04
C (%)	78.2 ± 0.71	71.5 ± 1.24	66.5 ± 0.12	71.8 ± 1.65
H (%)	3.7 ± 0.02	4.5 ± 0.41	3.2 ± 0.49	4.0 ± 0.19
O (%)	17.6 ± 0.75	23.4 ± 1.14	29.2 ± 0.27	24 ± 1.77
C:N	136.2 ± 3.64	120.5 ± 49.6	76.8 ± 32.34	452.8 ± 87.95
O:C	0.23	0.33	0.44	0.33
H:C	0.05	0.06	0.05	0.06
C:P	1.48	3.97	0.24	0.26
N:P	0.01	0.04	0.00	0.00
P (g kg^{-1})	52.78 ± 3.36	17.99 ± 0.95	273.57 ± 21.39	274.57 ± 20.03
K (g kg^{-1})	2.33 ± 0.16	4.27 ± 0.89	2.87 ± 0.08	4.20 ± 0.14
Na (g kg^{-1})	0.33 ± 0.08	0.93 ± 0.29	0.27 ± 0.14	0.40 ± 0.08
Cu (g kg^{-1})	0.01 ± 0.00	0.01 ± 0.00	0.01 ± 0.00	0.01 ± 0.00
Mn (g kg^{-1})	0.18 ± 0.01	0.08 ± 0.00	0.09 ± 0.00	0.08 ± 0.00
Mg (g kg^{-1})	0.70 ± 0.03	10.55 ± 0.18	10.85 ± 1.53	8.64 ± 0.81
Fe (g kg^{-1})	0.11 ± 0.04	2.66 ± 0.06	2.82 ± 0.07	2.31 ± 0.19
Ca (g kg^{-1})	10.58 ± 0.55	37.72 ± 3.37	39.27 ± 1.94	30.04 ± 2.17

and 19% higher compared to B2 (1.46 g pot^{-1}). The stimulus effect on sheath dry mass exhibited similar behavior to that for fresh mass, where the application of biochar B4 at the highest dose of 30 ton ha^{-1} (with biomass production of 0.25 g pot^{-1}) showed results close to that of the control (0.26 g pot^{-1}) and superior to those of the other treatments (Fig. 1e).

This behavior was also observed in the production of the fresh mass and dry mass of leaves. In the fresh and dry leaf biomass, only the application of 30 ton ha^{-1} B4 stimulated the production of the fresh mass (1.33 g pot^{-1}) (Fig. 1c) and dry mass of leaves (0.34 g pot^{-1}) (Fig. 1f) compared to the other biochars, but the effect was still lower than that of the control treatment (1.59 g pot^{-1} and 0.37 g pot^{-1}).

3.5 Effect of Biochar Application on Nutrient Accumulation in Rice Plant Tissues

Figure 2 shows the concentrations of macro- and micronutrients accumulated in the aerial parts of plants grown in soils supplemented with the different biochars. All biochars at all application doses in sandy soil promoted increases in plant P concentration. The plants grown in soil treated with biochar B3 showed the highest concentrations of P. B3 at all three doses (10, 20, and 30 ton ha^{-1}) promoted significantly more P accumulation (20.22 g kg^{-1}, 18.21 g kg^{-1}, and 21.22 g kg^{-1}) than the control (11.18 g kg^{-1}) (Fig. 2a). However, the B2 treatment at all three doses promoted more P accumulation in rice plants, mainly at the dose of 30 ton ha^{-1} (23.41 g kg^{-1}) than the control treatment (11.18 g kg^{-1}).

The K concentrations in plant tissues for the different treatments are shown in Fig. 2b. Biochar B1 promoted increases in plant K concentration of 25.89%, 26.25%, and 26.97% at doses of 10 ton ha^{-1}, 20 ton ha^{-1}, and 30 ton ha^{-1}, respectively, relative to the control. The application of B2 also increased K uptake by plants, with all doses showing concentrations significantly higher than the control, by between 8.27 and 18.70%. B3 promoted plant K uptake than the control only at doses of 10 ton ha^{-1} and 20 ton ha^{-1}, with increases of up to 11%. For B4, the accumulation of K was similar to that in the control treatment, with K contents of 28.7 g kg^{-1}, 28.2 g kg^{-1}, and 29.9 g kg^{-1} at doses of 10, 20, and 30 ton ha^{-1}, while in the control, the content was 28.4 g kg^{-1}. The application of treatments did not provide a significant increase in the Ca content in the aerial part of the plants (9.6 g kg^{-1}) (Fig. 2c). B1 resulted in the accumulation of an average of 10 g kg^{-1} of K at all doses applied. B2 caused lower plant Ca uptake when applied at a dose of 20 ton ha^{-1} (10.1 g kg^{-1}). When B3 and B4 were applied, Ca concentration did not increase compared to the control, with the highest concentration being with B3 in the dose 10 ton ha^{-1} (9.5 g kg^{-1}).

Plant Mg concentrations also showed a reduction compared to the control treatment (Fig. 2d). The treatments with B2 and B3 showed similar behavior, where, in both cases, concentrations of 10 ton ha^{-1} and 30 ton ha^{-1} resulted in the lowest Mg levels compared to the control. The opposite behavior was observed for B1, where the dose of 20 ton ha^{-1} caused the greatest reduction in Ca uptake. B4 caused the least reduction in Ca uptake by the plant at the dose of 30 ton ha^{-1} (2.6 g kg^{-1}), compared to the control (3.7 g kg^{-1}).

The amount of Cu absorbed and accumulated in plants with the application of biochar is shown in Fig. 2e. B2 showed the greatest reduction in plant Cu uptake for all three doses, with a decrease of up to 25% relative to the control. B3 at doses of 10 ton ha^{-1} and 20 ton ha^{-1} resulted in a decrease of up to 50% compared to the control. Biochar B4 promoted a decrease in Cu absorption at all doses, with reductions of up to 20% compared to the control treatment. B1 applied at the three concentrations resulted in a similar effect to the control treatment, where plants treated with 10 ton ha^{-1} showed the lowest accumulation compared to those treated with 20 ton ha^{-1} and 30 ton ha^{-1}.

The accumulation of Fe in plant tissues was reduced by the application of biochar (Fig. 2f). B4 at 20 ton ha^{-1} and 30 ton ha^{-1} caused a significant decrease in Fe absorption of up to 46% compared to the control treatment. The application of B2 at concentrations of 20 ton ha^{-1} and 30 ton ha^{-1} decreased Fe uptake by up to 44% compared to the control treatment. The highest Fe content was found with the addition of 20 ton ha^{-1} of biochar B1 (0.29 g kg^{-1}). For B2, the highest concentration of 30 ton ha^{-1} caused the greatest reduction in Fe uptake (0.16 g kg^{-1}).

The uptake of Zn by plants was strongly impaired by the application of biochar to the soil (Fig. 2g). B4 promoted the most intense reductions in plant Zn uptake at each applied dose, with reductions of up to 55% at the dose of 30 ton ha^{-1}. B4 promoted a decrease in Zn uptake at doses of 20 ton ha^{-1} and 30 ton ha^{-1} (0.18 and 0.20 g kg^{-1}), compared to the control (0.37 g kg^{-1}). B3 also caused significant reductions in Zn absorption, especially at 30 ton ha^{-1} (0.20 g kg^{-1}).

The Mn accumulation behavior under biochar application was highly variable (Fig. 2h). The application of B1 at a dose of 30 ton ha^{-1} significantly impaired Mn accumulation by up to 45% compared to the control. B2, also at the highest concentration, caused a significant reduction in Mn accumulation by up to 27% compared to the control treatment. All doses of B3 caused similar limitations in Mn accumulation, with a slight difference for the dose of 20 ton ha^{-1}, which showed a significant reduction in absorption of greater than 50% compared to the control. B4 at a concentration of 10 ton ha^{-1} resulted in an accumulation effect similar to that of the control treatment and was the only treatment that did not strongly inhibit Mn accumulation.

Fig. 1 Biomass of rice plants grown under different conditions: control treatment (red), application of artisanal biochar 1 (B1), artisanal biochar 2 (B2), artisanal biochar 3 (B3), and artisanal biochar 4 (B4), at doses of 10 t ha^{-1} (green), 20 t ha^{-1} (blue), and 30 t ha^{-1} (purple). Biochars with the same capital letter within each dose level are not significantly different according to Tukey's test ($p < 0.05$). Doses with the same lowercase letter within each biochar level are not significantly different according to Tukey's test ($p < 0.05$)
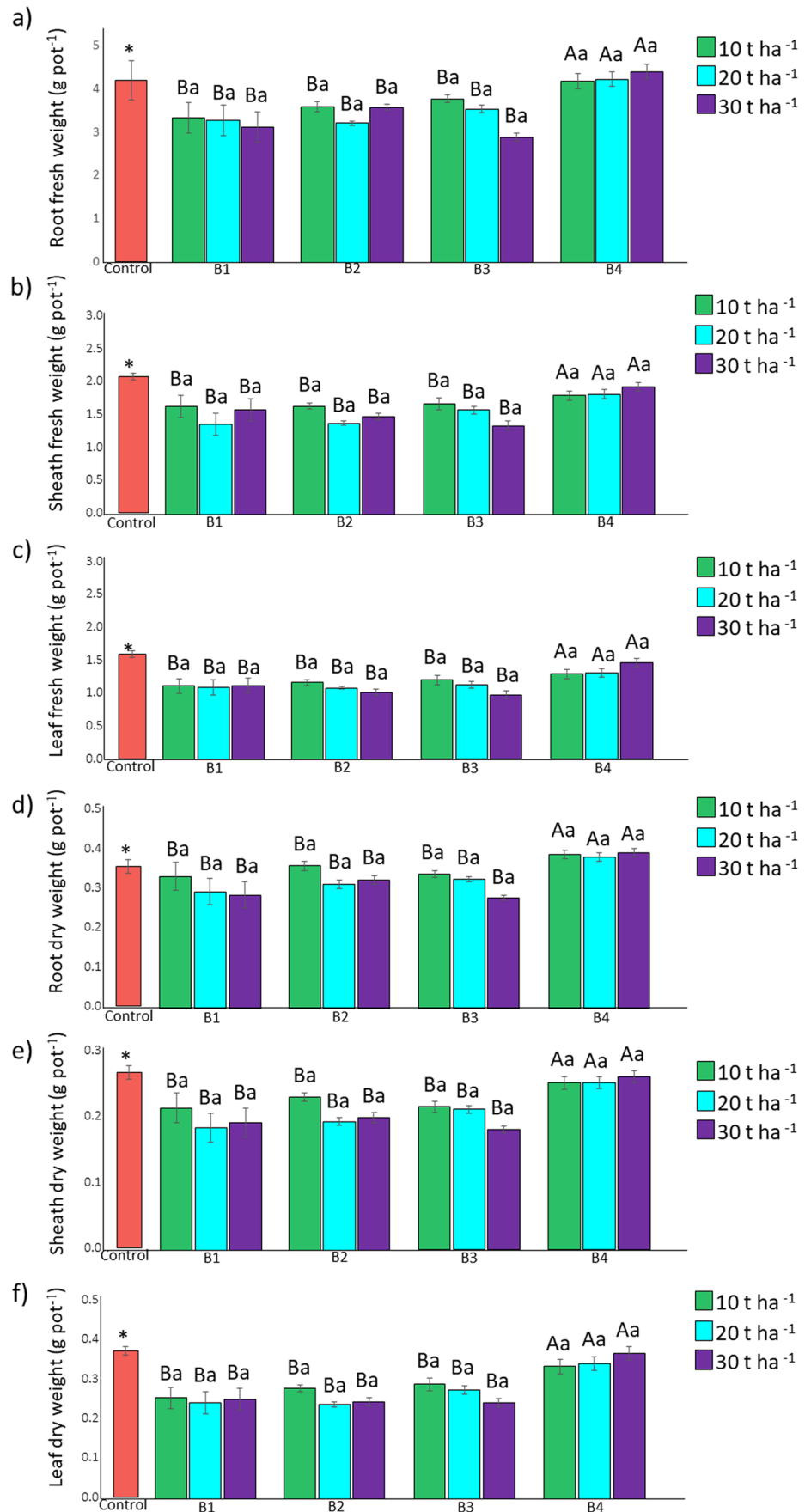
Fig. 2 Macro- and micronutrient concentrations in rice plants grown in soil under different conditions: control treatment (red), application of artisanal biochar 1 (B1), artisanal biochar 2 (B2), artisanal biochar 3 (B3), and artisanal biochar 4 (B4), at doses of 10 t ha^{-1} (green), 20 t ha^{-1} (blue), and 30 t ha$^{-.1}$ (purple). Biochars with the same capital letter within each dose level are not significantly different according to Tukey's test ($p < 0.05$). Dose with the same lowercase letter within each biochar level are not significantly different according to Tukey's test ($p < 0.05$)
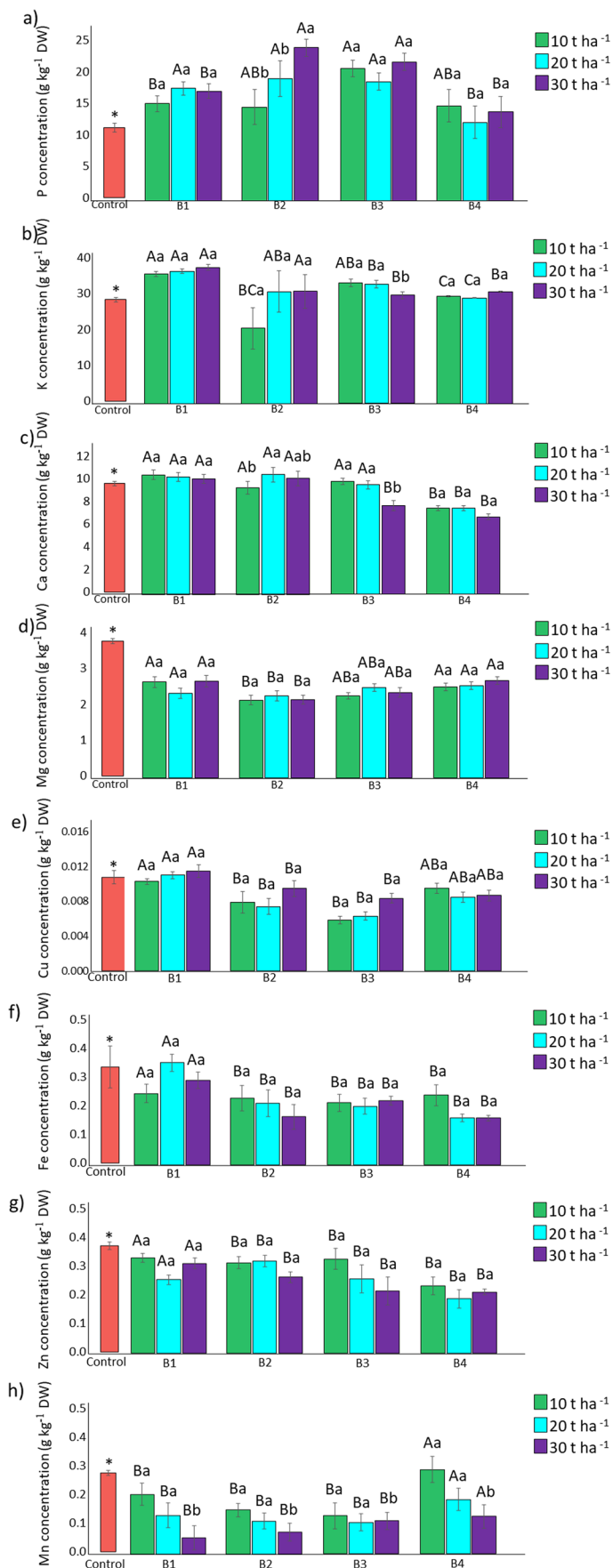
3.6 Effects of Biochar Application on the Transient Fluorescence Emission of Chlorophyll *a*

The photosynthetic parameters of the treated rice plants were obtained using the JIP test of the transient fluorescence of chlorophyll *a*, and the data were normalized with reference to the control. The analyses were performed 26 and 32 DAS. At 26 DAS, significant changes in photosynthetic parameters were noted in all treatments at different doses when compared to the control (Fig. 3a–d).

Treatment with B1 at the highest dose (30 ton ha^{-1}) promoted an increase in the plant photosynthetic performance index expressed on an absorption basis (PI$_{ABS}$) describing the conservation of excitation energy for the reduction of intersystem electron acceptors. This reduction was also observed in B2 (10 and 30 ton ha^{-1}) and B4 (30 ton ha^{-1}). A significant increase in the photosynthetic performance index describing the conservation of excitation energy for the reduction of the final acceptors of photosystem I (PSI) (PI$_{TOTAL}$) was observed in the treatments with B4 (30 ton ha^{-1}) and B3 (10 ton ha^{-1}). The increases in PI$_{ABS}$ and PI$_{TOTAL}$ indicate better functionality of the electron transport chain in the plants (Souza 2022).

The quantum yield of electron transport from QA- to intersystem electron acceptors (φEo) and the quantum yield of electron transport from QA- to the final electron acceptors of PSI (φRo) had significant increases under the treatments with B4 (30 ton ha^{-1}) and with B3 (10 ton ha^{-1}). Biochar B4 also resulted in significant increases in the specific activity per reaction center (RC); the electron capture (trapped energy) per RC (TR$_o$/RC); the electron transport per active RC, which can lead to the reduction of quinone A (QA-) (ET$_O$/RC); the flow of electrons to the final acceptors of PSI per RC (RE$_O$/RC); the energy loss in the form of heat (dissipated energy) per RC (DIo/RC); and the average antenna size per RC (ABS/RC).

However, at 32 DAS, the changes in the parameters were less intense, indicating re-establishment of the photosynthetic activities of the plants grown in soil treated with biochar when compared to the control (Fig. 3e–h). It is noteworthy that, even at 32 DAS, plants grown in soil treated with B4 at 30 ton ha^{-1} (Fig. 3h) also showed increases in PI$_{ABS}$ and PI$_{TOTAL}$, demonstrating higher photosynthetic performance. An increase in PI$_{ABS}$ was observed with 20 ton ha^{-1} B3 (Fig. 3g), but to a lesser extent. At the lowest doses of B4 (Fig. 3h) and at all doses of B2 (Fig. 3f), there was a reduction in PI$_{ABS \ and}$ PI$_{TOTAL}$, indicating a reduction in the photosynthetic efficiency of these plants.

Figure 4 shows the graphs of the transient fluorescence of chlorophyll *a* normalized to the relative variable fluorescence (OJIP curve; the points O (50 μs), J (2 ms), I (30 ms), and P (1 s) are marked) (Wt); the relative variable fluorescence normalized between O (50 μs) and I (30 ms) (WOI); and the relative variable fluorescence normalized between I (30 ms) and P (1 s) (WIP). In the graphs of the transient chlorophyll *a* fluorescence, an OJIP standard curve (Wt) was observed; however, in the treatment with B4 (Fig. 4j) at doses of 10 ton ha^{-1} and 30 ton ha^{-1}, a significant reduction between points J and I was observed. The WOI graph also showed a significant increase for the same treatment. The WIP graph (Fig. 4l) shows that the application of 30 ton ha^{-1} B4 reduced the relative variable fluorescence (normalization between points I (30 ms) and P (1 s)), thus reducing the sequence of electron transfer events from PSI to final acceptors. This was also observed at the lowest doses of B4 (Fig. 4l), at 10 ton ha^{-1} B1 and B3 (Fig. 4c, i) and at 30 ton ha^{-1} B3 (Fig. 4i), but in smaller proportions. However, this index increased only slightly with the application of 30 ton ha^{-1} B1 (Fig. 4c) and 10 ton ha^{-1} B2 (Fig. 4f). At 32 DAS, no significant changes were observed in the parameters evaluated.

Figure 5 shows the presence of L-bands (ΔW$_{OK}$) and K-bands (ΔW$_{OJ}$) at 26 DAS. Positive values were observed in the K-band (ΔWOK) in the treatments with 10 and 20 ton ha^{-1} B1 (Fig. 5a), 30 ton ha^{-1} B2 (Fig. 5b), 10 and 30 ton ha^{-1} B3 (Fig. 5c), and 10 and 30 ton ha^{-1} B4 (Fig. 5d). This band is associated with the activity of the oxygen evolution complex (OEC) (Ayyaz et al. 2020). These positive K-band values indicate that the plants were under stress, since as the data are normalized, plants under favorable conditions would not exhibit K-band deviation (Oukarroum et al. 2007; Tomek et al. 2001). The positive K band present in almost all treatments may reflect inhibition of the OEC, which is consistent with the fact that the donor side of photosystem II is inhibited (Pospíšil and Dau 2000; Tomek et al. 2001). This occurs because the transfer of electrons from the EOC to Yz is slower that from P680 to Q$_A$, which results in the emergence of the K-band. In this sense, when there is a condition (possible stress) that affects the capacity of the donor side, the K-band appears (Strasser 1997). Positive values of the L-band were also observed in all treatments (Fig. 5b, d, f, and h), which indicates low energy connectivity between the systems (ΔWOJ) (Ayyaz et al. 2020; Yusuf et al. 2010).

At 32 DAS, a reduction in the K-band was observed in all treatments (Fig. 5i, k, m, and o). This reduction indicates that the plant stress decreased, which may be related to the fertilization performed 25 DAS. After fertilization, the plants responded positively again, indicating nutritional stress, which was evidenced by the emergence of the K-band. The reduction in the positive L-band from the second sampling (Fig. 5j, l, n, and p) indicates that the system was stable in terms of energy connectivity and efficient consumption of excitation energy (De Souza et al. 2020).
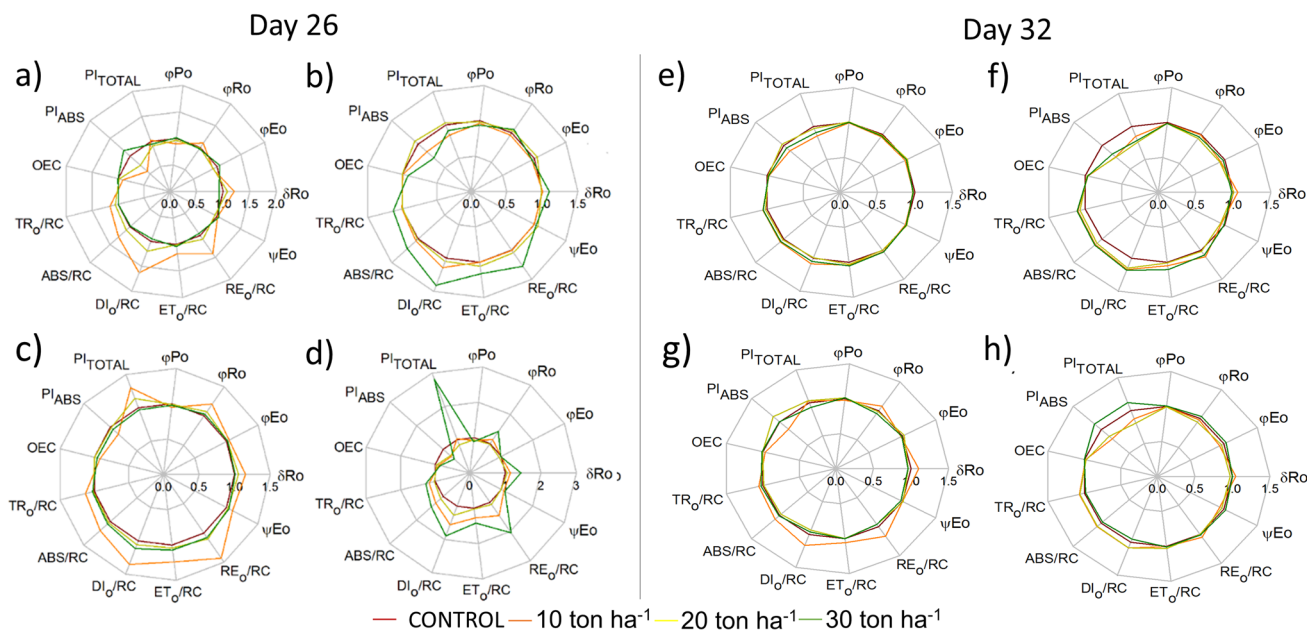
Fig. 3 Analysis of the photosynthetic parameters of rice plants with different biochars by the JIP transient fluorescence test normalized using the control as a reference. **a** Artisanal biochar 1 (B1) at 26 days; **b** artisanal biochar 2 (B2) at 26 days; **c** artisanal biochar 3 (B3) at 26 days; **d** artisanal biochar 4 (B4) at 26 days; **e** artisanal biochar 1 (B1) at 32 days; **f** artisanal biochar 2 (B2) at 32 days; **g** artisanal biochar 3 (B3) at 32 days; **h** artisanal biochar 4 (B4) at 32 days; at doses of 10 t ha^{-1} (orange), 20 t ha^{-1} (yellow), and 30 t ha.$^{-1}$ (red)

3.7 Effects of Biochar Application on the Root Morphology of Rice Plants

The application of biochar to the soil promoted changes in the root morphology of rice plants (Fig. 6). The total root area was stimulated mainly by the application of B4 (Fig. 6a) and increased by 25% and 26% compared to the control group; however, there was no significant difference between the treatment doses. The contribution to area of the different root classes was different; however, treatment with B4 had the greatest influence. The area of superfine roots (Fig. 6b) showed the greatest stimulus by B4, increasing by approximately 55% (10 ton ha^{-1}) and 56% (20 ton ha^{-1} and 30 ton ha^{-1}) compared to the control. A significant difference was also observed in the contribution of the fine root area (Fig. 6c), but with a greater influence of the 20 ton ha^{-1} dose, which resulted in a 51% increase compared to the control. The contribution of the thick root area (Fig. 6d) for the B4 treatment was also significantly higher than the control, but the proportions were lower than those for other root classes; a 15% increase was observed, with no significant difference between doses.

The total root length was also significantly influenced by the application of biochar (Fig. 6e). The application of B4 at the three doses provided a significant increase of 47 and 48% in total root length at all doses; moreover, 30 ton ha^{-1} B2 promoted a 27% increase compared to the control. Superfine roots were highly affected by the application of B4, with increases in root length of 67% (20 ton ha^{-1}) and 66% (10 and 30 ton ha^{-1}) (Fig. 6f). The dose of 30 ton ha^{-1} also provided a 38% increase in the length of superfine roots. For fine roots, 20 ton ha^{-1} B4 increased root length by 53%, while the doses of 10 ton ha^{-1} and 30 ton ha^{-1} increased root length by 52%, and 30 ton ha^{-1} B2 stimulated root length by up to 26% (Fig. 6g). The impact of B4 on the length of thick roots was considerably lower, resulting in an increase of approximately 11% compared to the control (Fig. 6h).

The total root volume was less affected by the treatments, increasing by up to 7% for all doses of B4 (Fig. 6i), 50% for the volume of superfine roots (Fig. 6j), and 33% for the volume of fine roots (Fig. 6k) compared to the control. For thick root volume (Fig. 6l), the treatments showed no significant difference compared to the control. In contrast, the total number of spikes (Fig. 6m) was strongly influenced by the application of B4: an increase of 65% was observed for all doses, with a consistent impact on superfine roots (Fig. 6n), fine roots, and coarse roots (Fig. 6o, p). The total number of forks (Fig. 6q) exhibited similar behavior to the other parameters, with a greater influence of B4. However, the root diameter (Fig. 6r) exhibited different behavior, with a greater influence of B1, which caused a slight increase of 9% at the dose of 20 ton ha^{-1} and 8% at the dose of 30 ton ha^{-1}.
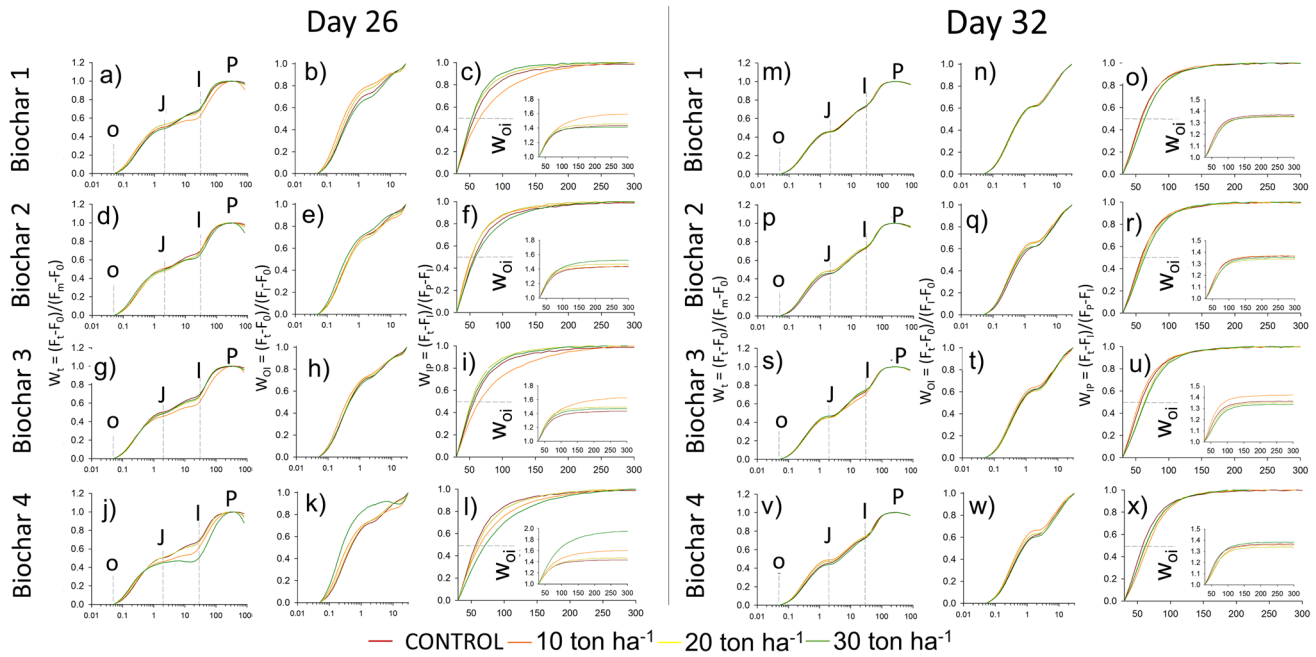
Fig. 4 Transient chlorophyll a fluorescence in dark-adapted leaves of rice plants (*Oryza sativa* L.) cultivated under different conditions. Relative variable fluorescence between points O and P (Wt) on a logarithmic time scale (**a**, **d**, **g**, **j**, **m**, **p**, **s**, and **v**); relative variable fluorescence between points O and I (WOI) on a logarithmic time scale (**b**, **e**, **h**, **k**, **n**, **q**, **t**, and **w**); relative variable fluorescence between points I and P (WIP) and WOI in the inset (**c**, **f**, **i**, **l**, **o**, **r**, **u**, and **x**)

3.8 Relationship Between the Parameters Evaluated by Multivariate PCA

Figure S5 shows the relationships between the variables obtained by PCA, which clarify the relationship between each biochar used and its effects on plants. B4 promoted P accumulation in plants (negative PC-1 values, 28.7% of explained variance) as well as higher amounts of Mn, Mg, Fe, and Cu (negative PC-2 values, 22.1% of explained variance) (Fig. S5a). B4 also stimulated root parameters (positive PC-1 values, 79.3% of explained variance) more than the control treatment (Fig. S5b) and better maintained the production of root biomass than B1, B2, and B3 (positive values of PC-1, 84.1% of explained variance) (Fig. S5c). B4 has structural characteristics that generate more balanced chemical properties compared to other biochars, such as aromaticity, aliphaticity, and an intermediate hydrophobicity index.

B3 has compositional and structural characteristics similar to those found in B4 (negative PC-1 values, 28.7% of explained variance), promoting a nutrient accumulation effect that was also similar to that of B4 (Fig. S5a). However, these biochars exhibited notable differences: the C:N ratio was the lowest of all biochars, the O:C ratio was the highest of all biochars (Table 1), and the contents of -C$_{COOH}$ and -C$_{C=O}$ were greater (Fig. S4d1-d3). These differences were

sufficient to limit the stimulation effects on root morphology (negative PC-1 values, 79.3% of explained variance) (Fig. S5b) as well as on the growth and development of rice plants (negative PC-1 values, 84.1% of explained variance) (Fig. S5c).

B2 showed compositional characteristics different from those found in B4 and B3, with the lowest amount of P, the second highest amounts of Ca, Fe, and Mg, and the highest amounts of Na and K. P was more efficient when compared to the other biochars (positive PC-1 values, 28.7% of explained variance) (Fig. S5a). Biochar B2 is structurally the most aliphatic among all the biochars (Fig. S4d2). As a result of these characteristics, B2 inhibited root morphology development (negative PC-1 values, 79.3% of explained variance) (Fig. S5b) and biomass production in rice plants (negative PC-1 values, 84.1% of explained variance) (Fig. S5c).

B1 has a lower amount of P than B3 and B4 and has the lowest amounts of K, Mg, Fe, and Ca (Table 1). B1 is also the biochar with the highest hydrophobicity index. These traits limited the accumulation of nutrients, especially K, Ca, and Zn, by the plants (positive values of PC-1, 28.7% of explained variance) (Fig. S5a). Biochar B1 most strongly inhibited root growth and development (negative PC-1 values, 79.3% of explained variance) (Fig. S5b) as well as the production of biomass in rice plants (negative PC-1 values, 84.1% of explained variance) (Fig. S5c).
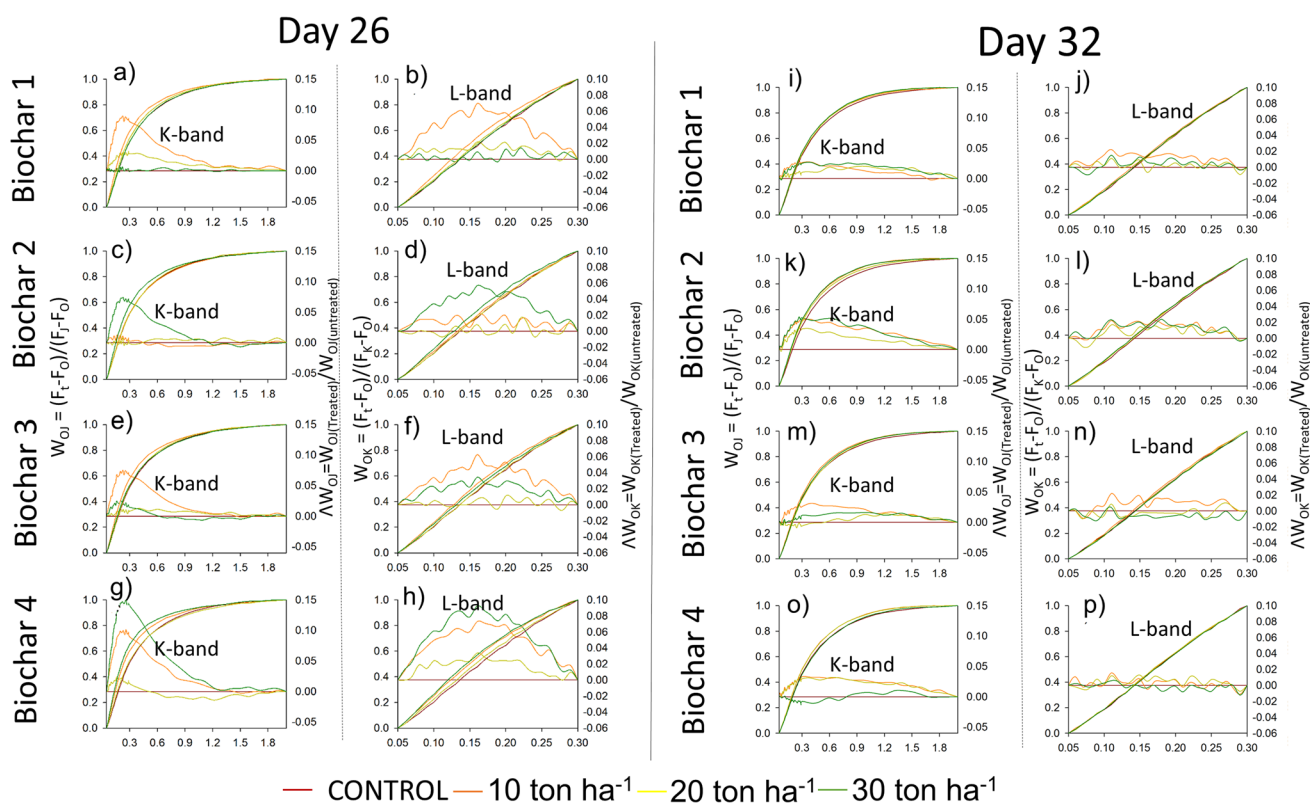
Fig. 5 Relative variable fluorescence between points O and J (WOJ; left vertical axis and graph with symbols) and mean kinetics (right vertical axis and graph without symbols) between points O and J (ΔWOJ), revealing the K band (a, c, e, g, i, k, m, and o); relative vari- able fluorescence between points O and K (WOK; left vertical axis and graph with symbols) and mean kinetics (right vertical axis and graph without symbols) between points O and K (ΔWOK), revealing the L band (b, d, f, h, j, l, n, and p)

4 Discussion

A high carbon content indicates biochar with greater recalcitrance because it has a greater number of aromatic rings in its structure (Feitosa et al. 2020). Low N concentration in biochars may be attributed to the volatilization of nitrogenous compounds during the thermal degradation process. However, it is important to note that N can still be present in biochars even after pyrolysis. During pyrolysis, various structural and chemical changes take place, leading to the transformation of nitrogen from more readily available organic forms, such as protein-N, free amino acid-N, and alkaloid-N, to more stable chemical forms such as nitrile-N, pyridine-N, amino-N, and pyrrole-N, as well as inorganic forms like NH_4^+-N, NO_2-N, and NO_3^--N (Liu et al. 2018). Additionally, research by Chen et al. (2018) indicates that a restructuring reaction can occur during pyrolysis, allowing nitrogen to stabilize in various structural configurations, including include pyridinic-N, pyrrolic-N, quaternary-N, and pyridine-N-oxide. The low O and H contents are consistent because pyrolysis causes water loss and hydrocarbon volatilization, decreasing the contents of these elements (Torchia et al.

2021). In addition, low values of O and H may be associated with greater biochar hydrophobicity due to the lower content of heteroatomic functional groups. The low O:C and H:C ratios indicate that, even under artisanal conditions, structural transformation and loss of hydrophilic functional groups occurred during the pyrolysis process (Pradhan et al. 2020). The N:P ratio affects how efficiently N and P are used in plant growth; therefore, changes in this ratio influence physiological mechanisms (Güsewell 2004; Zhang et al. 2013. On the other hand, high C:P and N:P ratios mainly indicate P limitation (Huang et al. 2018). The PCA revealed possible interactions in the soil due to the composition of the different biochars. B3 contains oxygenated groups in its structure, as well as higher amounts of metals such as Fe. These chemical conditions are conducive to the formation of inner-sphere complexes with P, promoting high P availability to plants. Studies have described the modification of biochar with metals to retain P in the biochar structure (Wu et al. 2019, 2020; Yin et al. 2018). Additionally, Fe oxides effectively combine with P through complexation with surface ions. Therefore, the binding of two surface hydroxyl ions is altered by the addition of a phosphate ion, forming a stable complex (Parfitt et al. 1975; Wu et al. 2020). For
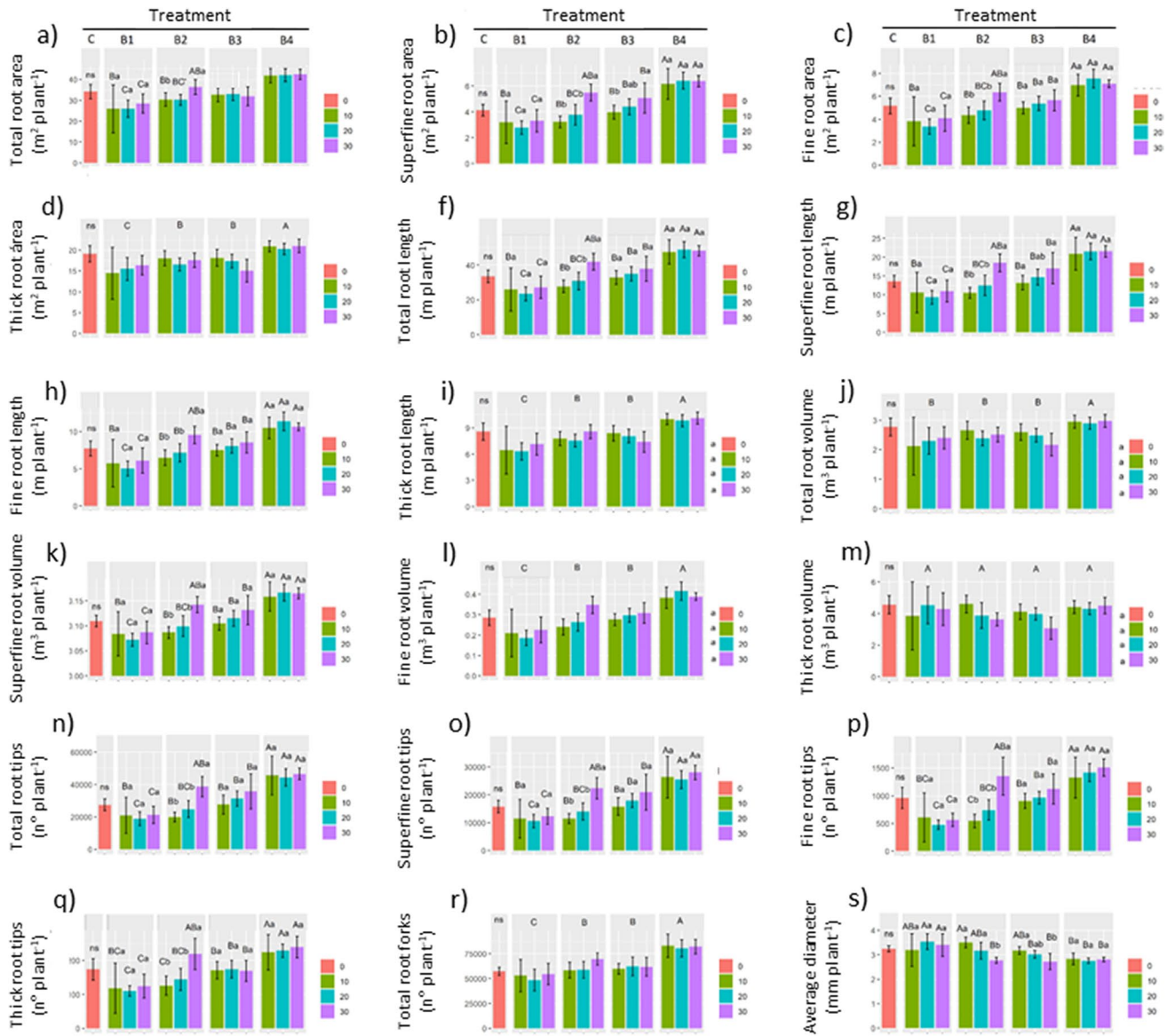
Fig. 6 Root morphology of rice plants cultivated with in soil under different conditions: control treatment (red), application of artisanal biochar 1 (B1), artisanal biochar 2 (B2), artisanal biochar 3 (B3), and artisanal biochar 4 (B4), at doses of 10 t ha^{-1} (green), 20 t ha^{-1} (blue), and 30 t ha.$^{-1}$ (purple). Biochars with the same capital let-ter within each dose level are not significantly different according to Tukey's test ($p < 0.05$). Doses with the same lowercase letter within each biochar level are not significantly different according to Tukey's test ($p < 0.05$)

the studied soil, biochar with these characteristics is of interest because in Planosols, even if present, phosphorus (P) is often unavailable to plants due to its fixation. P fixation occurs through the formation of an inner sphere complex, in which orthophosphate ions replace hydroxyl groups on the surface of aluminum or iron oxides, hydroxides, or the clay surface. Following this reaction, the possibility of P being desorbed into the soil solution is extremely low as it becomes an integral part of the oxide mineral (Idris and Ahmed 2012; Johan et al. 2021). According to Johan et al. (2021), the integrated use of soil improvers such as biochar not only increases P availability but also enhances P use efficiency in acidic soils. This is because negatively charged functional groups present in charcoal organic substances can interact with positively charged aluminum and iron oxides, thereby altering P sorption in soils.

In contrast, the more aromatic and less functionalized structure observed in B4 and the lower presence of metals could reduce interactions with P, preventing fixation processes and probably limiting availability. According to the above analyses, B4 may be promising for plant development when applied to sandy soil with a low nutrient content, especially a low P content. These issues were evaluated in the bioactivity tests performed in this study.

The peaks in C_{alkyl} and C_{alkyl}-O were weaker in B2 and stronger in B4, and they correspond to polysaccharides such as cellulose and hemicellulose (Bonanomi et al. 2018; Kogel-Knabner 2002). This peak signal commonly has high intensity in plant residues rich in cutin and wax (Preston et al. 2009). Therefore, although the biomass and production conditions of the investigated materials are unknown, because they are artisanal biochars, it can be assumed that the materials are derived from vegetable raw material composed of predominantly aliphatic groups, which were reduced in the production process. This reduction is consistent with previous studies on plant residues and the influence of pyrolysis on biochar molecules (Bonanomi et al. 2015, 2018; Xiao et al. 2016). All artisanal biochars showed the predominance of aromatic carbon. Increased thermal degradation induces the dehydration and selective degradation of carbohydrate and protein structures, adding recently formed aromatic constituents (García et al. 2019). There is strong evidence that this region is particularly intense in biochar produced at high temperatures (Bonanomi et al. 2018; He et al. 2020; Torchia et al. 2021). Therefore, it is likely that biochar B2 was produced at temperatures lower than those of the other biochars. Das et al. 2023 reported that biochar produced at 600 °C demonstrated the strong C=C aromatic carbon structure with negligible C=O/OH or -OH groups.

The data reveal that the biomass production was mainly influenced by the application of B4 and increased with increasing dose, resulting in increases of up to 26% in the root, sheath, and leaf mass when compared to those obtained with the other biochars. A similar increase of 29% was also obtained in a study with application of 30 ton ha^{-1} of rice husk biochar in rice biomass production (Miao et al. 2023). The effects of soil biochar application on plant biomass production are still contradictory. Several studies have shown that the application of biochar increases the production of aerial biomass, especially when the dose is increased (Dietrich et al. 2020; Silva Gonzaga et al. 2019). However, inhibitory effects were also observed in the production of *ryegrass* (Jeffery et al. 2011), *Lepidium* and *Brassica* (Marra et al. 2018). Biochar can affect plant performance in terms of both germination and growth. A meta-analysis study reported that the application of biochar increases plant yield by approximately 10 to 42% when the dose is in the range of 5–20 ton ha^{-1}. A recent study revealed that a low concentration of biochar significantly increased iron plaque formation due to direct oxidation or electron transfer of Fe(II). However, when biochar was applied in excess, it not only negatively affected iron plaque formation but also impaired plant growth and nutrient uptake (Gu et al. 2022). These results corroborate the negative effects of B1, B2, and B3 on rice growth, as observed in this study.

Several studies have reported that the application of biochar to soil promotes an increase in macronutrients in the aerial parts of plants; this result was also observed in this study, especially in the case of P, K, and Ca (Schmidt et al. 2017; Xu et al. 2022). However, there are also reports that corroborate the results of this study, in which the application of biochar did not show promising results in increasing nutrient uptake, especially when biochar was applied to fragile soils that do not have nutrient concentrations conducive to plant development (Huang et al. 2020).

As observed in this study, several parameters, such as the dose, the raw material, the conditions of biochar production, and the nutritional requirements of various crops, influence the effects of biochar on plants. Reports have shown that biochar produced from firewood reduces the concentration of micronutrients (Fe, Mn, Cu, and Zn) in wheat grains (Hartley et al. 2016). On the other hand, woody biochar increased Fe and Zn adsorption in legumes and vegetables (Gao et al. 2016). Moreover, the use of wheat straw biochar reduced the Mn concentration in the aerial parts of maize but did not reduce the concentration of Fe (Bornø et al. 2019). Therefore, even if the increase in nutrients in plant aerial parts is minor, the application of biochar to soil is still an effective amendment since it affects not only nutritional components but also other soil parameters, such as water retention and carbon content, which contribute to plant development and soil regeneration.

The observed changes in the parameters of the JIP test at 26 DAS (Fig. 3a–d) compared to the control indicate changes in structural and functional parameters related to the photosynthetic behavior of the plants treated with biochar. The changes in PI_{ABS} and PI_{TOTAL}, as well as the increases in φEo, φRo, TR_0/RC, ETO/RC, DIo/RC, and ABS/RC, indicate physiological responses of the plants to stress events. The positive values of the K-band observed in Fig. 5 corroborate this finding, indicating that the plants were under stress (Oukarroum et al. 2007; Tomek et al. 2001). However, the re-establishment of the photosynthetic parameters of the JIP test, the relative variable fluorescence, and the K-bands and L-bands (Figs. 3, 4, and 5) after mineral fertilization of the soil (32 DAS) suggest that the stress observed at 26 DAS may indicate a nutritional deficiency promoted by the application of the different biochars studied. Interestingly, plants grown in soils that received biochar B3 (10 ton ha^{-1}) and B4 (30 ton ha^{-1}) showed a significant increase in photosynthetic performance at 26 DAS, which was maintained at a lower intensity at 32 DAS. B3 and B4 exhibit structural similarity,

as confirmed by PCA analyses of their FTIR and NMR spectra (Figs. 3b and 4b). B3 and B4 also presented higher phosphorus and oxygen content and therefore a greater presence of oxygenated functional groups. These chemical and structural characteristics of B3 and B4 allowed the maintenance of photosynthetic metabolism in rice plants, although under suboptimal nutritional conditions. The soil characteristics favored by the addition of biochar B3 and B4 contributed to a reduction in fluorescence (Fig. 3), mainly between points J and P of the transient curve. Greater changes were indicated in the sequence of electron transfer by PSI to the final electron acceptors, starting at PQH_2 (plastoquinol) (W_{IP}), in addition to increases in the photosynthetic performance indices PI_{ABS} and PI_{TOTAL}. Wang et al. (2021) demonstrated that the application of 10 and 20 ton ha^{-1} of biochar improved the proportion of open PSII reaction centers and the photosynthetic electron transfer rates in peanut leaves. In addition, a reduction in heat dissipation was observed, which allowed the maximum use of light energy absorbed by the leaves for photosynthesis, consequently increasing peanut production.

Roots play a crucial role in the conversion and cycling of nutrients in the soil–plant system. The application of the studied biochars promoted better root development, increasing all the morphological parameters evaluated (area, length, volume, tips, forks, and average diameter). Several studies show that the porous structure and physical–chemical characteristics of biochars produce effects on roots. For example, the addition of biochar significantly reduces the bulk density of the soil while increasing the total porosity, providing ample space for roots to grow and facilitating their penetration and extension (Oguntunde et al. 2008). Biochar generally has an alkaline nature, which can raise soil pH, thus favoring root development, especially in acidic soils such as the studied Planosol (Chang et al. 2021; Kartika et al. 2021; Purkaystha et al. 2022). Furthermore, the beneficial effects of biochar on microbiological activities may influence the rhizosphere environment and, consequently, root growth (Warnock et al. 2007). Other studies have also indicated that biochar can release small molecules, such as ethylene, or produce hormone-like substances (Fulton et al. 2013), which can affect root secretions, stimulating or interfering with the physiological processes of the roots. Previous studies also found a positive influence of biochar on root morphological parameters, increasing the volume, area, and length and reducing the average diameter of the roots compared to the control (Robertson et al. 2012).

The PCA of the structure–property-function relationships of biochar may indicate that in fragile soil with a sandy texture, the compositional and structural characteristics of the biochar determine the effects on plants in their initial growth phase. In structural terms, it was observed that extreme structural characteristics, such as high hydrophobicity and high aliphaticity, do not favor plant development in fragile sandy soils. Under these conditions, plant growth may be favored by biochar obtained under conditions that favor a greater balance of chemical properties and their various components. In compositional terms, in the studied biochars, there does not seem to be a relationship between high amounts of nutrients, at least for P, and nutrient availability to plants.

Several mechanisms are involved in the interaction of biochar with the soil and plants. The biochar applied to the soil has immediate effects. In the first 3 weeks after application to the soil, the water that enters the pores of the biochar dissolves soluble organic and mineral compounds on the external and internal surfaces of the biochar. These solutes increase dissolved organic carbon (DOC), cations, and anions in the soil solution (Silber et al. 2010), which increases electrical conductivity and pH and reduces Eh (Joseph et al. 2015). The composition of the soil solution depends on the specific biochar and the soil (Mukherjee and Zimmerman 2013; Schreiter et al. 2020). The release of DOC and nutrient ions from biochar (Kim et al. 2013) is fast in the first week and much slower in the following weeks (Mukherjee and Zimmerman 2013). Rapid initial dissolution can occur via salt dissolution, ion exchange, submicron particle detachment, and preferential dissolution into crystalline imperfections (Wang et al. 2020). After the initial stage of rapid dissolution, continuous dissolution is faster in acidic (Silber et al. 2010) and low-nutrient soils (Wang et al. 2020). With this information, even in a short-term experiment, it is possible to observe the initial action of the biochar and use this information to find a dose and a type of biochar that best influence plant development. With this prior information, it is possible to develop experiments over a longer period and apply more sophisticated analyses, which are expensive and difficult to access. Therefore, these short-term experiments are important.

In the context of process engineering, the contribution of this study is paramount. It serves as the foundation for a transformative process that can convert over 15 tons of previously discarded fine charcoal per week, a prevalent issue in the study's region. This conversion turns artisanal charcoal into biochar, a valuable resource with the potential for significant compositional enhancements. Moreover, this biochar can be further processed into an organo-mineral fertilizer specifically designed to address the challenges of low-fertility soils, particularly those with a sandy texture. Thus, the study's findings hold promise for not only reducing waste but also enhancing soil conditions and fostering sustainable agricultural practices in the region.

In agronomic terms, the studied artisanal biochars proved to be a promising alternative for small producers who seek to improve the conditions of Planosols for cultivation. Although the application of biochar did not result in an above-control yield, the benefits of biochar are important. It is noted that there was better availability of nutrients to the plants, reflected by the increase in the aerial part caused by the biochar treatments, in addition to the better development

of the roots. This evaluated short-term effect is important, as it serves as a starting point for approaches on the ground in question. More studies are still needed to elucidate the effects of biochar on Planosols, such as longer-term tests, different cultures, and analyses of soil parameters.

5 Conclusion

In conclusion, the studied biochars improved rice cultivation. Although the biomass production was not higher in most treatments compared to the control, there was a significant increase in the nutrient content of the aerial part, mainly with the application of B2. In addition, there were improvements in photosynthetic parameters and root morphology, with emphasis on the application of B4. In general, the results found in this study showed that biochars B2 and B4 at doses of 20 and 30 ton ha^{-1} are promising for improving cultivation in fragile Planosols in the region of Rio de Janeiro (Brazil). However, despite the demonstrated effects, long-term and large-scale research is needed to verify the effects on soil properties in different cultures and the economic impact of its implementation in agriculture.

Declarations

Competing Interests There authors declare no competing interests.

References

Antonangelo JA, Zhang H, Sun X, Kumar A (2019) Physicochemical properties and morphology of biochars as affected by feedstock sources and pyrolysis temperatures. Biochar 1:325–336. https://doi.org/10.1007/s42773-019-00028-z

Ayyaz A, Amir M, Umer S, Iqbal M, Bano H, Gul HS, Noor Y, Kanwal A, Khalid A, Javed M, Athar HR, Zafar ZU, Farooq MA (2020) Melatonin induced changes in photosynthetic efficiency as probed by OJIP associated with improved chromium stress tolerance in canola (Brassica napus L.). Heliyon 6:e04364. https://doi.org/10.1016/j.heliyon.2020.e04364

Bonanomi G, Incerti G, Cesarano G, Gaglione SA, Lanzotti V (2015) Cigarette butt decomposition and associated chemical changes assessed by 13C CPMAS NMR. PLoS ONE 10:1–16. https://doi.org/10.1371/journal.pone.0117393

Bonanomi G, Ippolito F, Cesarano G, Vinale F, Lombardi N, Crasto A, Woo SL, Scala F (2018) Biochar chemistry defined by 13C-CPMAS NMR explains opposite effects on soilborne microbes and crop plants. Appl Soil Ecol 124:351–361. https://doi.org/10.1016/j.apsoil.2017.11.027

Bornø ML, Müller-Stöver DS, Liu F (2019) Biochar properties and soil type drive the uptake of macro- and micronutrients in maize (Zea mays L.). J Plant Nutr Soil Sci 182:149–158. https://doi.org/10.1002/jpln.201800228

Chang Y, Rossi L, Zotarelli L, Gao B, Shahid MA, Sarkhosh A (2021) Biochar improves soil physical characteristics and strengthens root architecture in muscadine grape (Vitis rotundifolia L.). Chem Biol Technol Agric 8:1–11. https://doi.org/10.1186/s40538-020-00204-5

Chen W, Chen Y, Yang H et al (2018) Investigation on biomass nitrogen-enriched pyrolysis: influence of temperature. Bioresour Technol 249:247–253

Das SK, Ghosh GK (2022) Soil hydro-physical properties affected by biomass-derived biochar and organic manure: a low-cost technology for managing acidic mountain sandy soils of north eastern region of India. Biomass Convers Biorefin 1:1–15

Das SK, Ghosh GK (2022) Conversion of biomass into low-cost biochar along with organic manure improved soil hydro-physical environment through technological intervention for sandy soil restoration. Biomass Convers Biorefin 1:1–13

Das SK, Ghosh GK, Mishra VK et al (2021) Utilizing dissimilar feedstocks derived biochar amendments to alter soil biological indicators in acidic soil of Northeast India. Biomass Convers Biorefin 13:10203–10214

Das SK, Ghosh GK, Avasthe R (2022) Biochar and organic manures on produce quality, energy budgeting, and soil health in maize-black gram system. Arab J Geosc 15:1527

Das SK, Choudhury BU, Hazarika S et al (2023) Long-term effect of organic fertilizer and biochar on soil carbon fractions and sequestration in maize-black gram system. Biomass Convers Biorefin 1:1–14

de Souza CCB, Borella J, Leal JFL, Tornisielo VL, Pimpinato RF, Monquero PA, de Pinho CF (2020) Limited diclosulam herbicide uptake and translocation-induced tolerance in Crotalaria juncea. Bull Environ Contamin Toxicol 104:114–120. https://doi.org/10.1007/s00128-019-02742-7

Demetrio WC, Ribeiro RH, Nadolny H, Bartz ML, Brown GG (2020) Earthworms in Brazilian no-tillage agriculture: status and future challenges. Euro J Soil Sci 71:988–1005

Dietrich CC, Rahaman MA, Robles-Aguilar AA, Latif S, Intani K, Müller J, Jablonowski ND (2020) Nutrient loaded biochar doubled biomass production in juvenile maize plants (Zea mays L.). Agronomy 10:567. https://doi.org/10.3390/agronomy10040567

Dokoohaki H, Miguez FE, Laird D, Horton R, Basso AS (2017) Assessing the biochar effects on selected physical properties of a sandy soil: an analytical approach. Commun Soil Sci Plant Anal 48:1387–1398. https://doi.org/10.1080/00103624.2017.1358742

Feitosa AA, Teixeira WG, Ritter E, Resende FA, Kern J (2020) Characterization of biochar samples of banana peels and orange bagasse carbonized at 400 and 600°C. Rev Virtual de Quimica 12:901–912. https://doi.org/10.21577/1984-6835.20200072

Fulton W, Gray M, Prahl F, Kleber M (2013) A simple technique to eliminate ethylene emissions from biochar amendment in agriculture. Agron Sustain Dev 33:469–474

Gao S, Hoffman-Krull K, Bidwell AL, DeLuca TH (2016) Locally produced wood biochar increases nutrient retention and availability in agricultural soils of the San Juan Islands, USA. Agric Ecosyst Environ 233:43–54. https://doi.org/10.1016/j.agee.2016.08.028

García AC, Santos LA, de Souza LGA, Tavares OCH, Zonta E, Gomes ETM, García-Mina JM, Berbara RLL (2016) Vermicompost humic acids modulate the accumulation and metabolism of ROS in rice plants. J Plant Physiol 192:56–63. https://doi.org/10.1016/j.jplph.2016.01.008

García AC, Castro TAVT, Berbara RLL, Elias SS, Amaral Sobrinho NMB, Pereira MG, Zonta E (2019) Revisão sobre a relação estrutura-função das substâncias húmicas e a sua regulação do metabolismo oxidativo em plantas. Quím Nova 11:754–770

Gu S, Lian F, Han Y et al (2022) Nano-biochar modulates the formation of iron plaque through facilitating iron-involved redox reactions on aquatic plant root surfaces. Environ Sci Nano 9:1974–1985

Güsewell S (2004) N: P ratios in terrestrial plants: variation and functional significance. New Phytol 164:243–266. https://doi.org/10.1111/j.1469-8137.2004.01192.x

Hartley W, Riby P, Waterson J (2016) Effects of three different biochars on aggregate stability, organic carbon mobility and micronutrient bioavailability. J Environ Manage 181:770–778. https://doi.org/10.1016/j.jenvman.2016.07.023

He Z, Guo M, Fortier C, Cao X, Schmidt-Rohr K (2020) Fourier transform infrared and solid state 13 C nuclear magnetic resonance spectroscopic 3 characterization of defatted cottonseed meal-based biochars. Modern Appl Sci 15(1):108

Huang J, Wang P, Niu Y, Yu H, Ma F, Xiao G, Xu X (2018) Changes in C:N: P stoichiometry modify N and P conservation strategies of a desert steppe species *Glycyrrhiza uralensi*s. Sci Rep 8:12668. https://doi.org/10.1038/s41598-018-30324-w

Huang S, Wang P, Yamaji N, Ma JF (2020) Plant nutrition for human nutrition: hints from rice research and future perspectives. Mol Plant 13:825–835. https://doi.org/10.1016/j.molp.2020.05.007

Idris OA, Ahmed HS (2012) Phosphorus sorption capacity as a guide for phosphorus availability of selected Sudanese soil series. Afr Crop Sci J 20:59–65

Jeffery S, Verheijen FGA, van der Velde M, Bastos AC (2011) A quantitative review of the effects of biochar application to soils on crop productivity using meta-analysis. Agric Ecosys Environ 144:175–187. https://doi.org/10.1016/j.agee.2011.08.015

Johan PD, Ahmed OH, Omar L, Hasbullah NA (2021) Phosphorus transformation in soils following co-application of charcoal and wood ash. Agronomy 11:1–25

Joseph S, Husson O, Graber ER, Zwieten LV et al (2015) The electrochemical properties of biochars and how they affect soil redox properties and processes. Agronomy 5:322–340

Kartika K, Sakagami JI, Lakitan B, Yabuta S, Akagi I, Widuri LI, Siaga E, Iwanaga H, Nurrahma AHI (2021) Rice husk biochar effects on improving soil properties and root development in rice (*Oryza Glaberrima* Steud.) Exposed to drought stress during early reproductive stage. AIMS Agric Food 6:737–751. https://doi.org/10.3934/AGRFOOD.2021043

Kim P, Johnson AM, Essington NME, Radosevich M, Kwon WT, Lee SH, Rials TG, Labbé N (2013) Effect of pH on surface characteristics of switchgrass-derived biochars produced by fast pyrolysis. Chemosphere 90:2623–2630

Kogel-Knabner I (2002) The macromolecular organic composition of plant and microbial residues as inputs to soil organic matter. Soil Biol Biochem 34:139–162

Lehmann J, Joseph S (2015) Biochar for environmental management: an introduction. Routledge, London

Li L, Zhang YJ, Novak A, Yang Y, Wang J (2021) Role of biochar in improving sandy soil water retention and resilience to drought. Water (switzerland) 13:407. https://doi.org/10.3390/w13040407

Liu Y et al (2018) Impact of biochar amendment in agricultural soils on the sorption, desorption, and degradation of pesticides: a review. Sci Total Environ 645:60–70

Lopes WA, Fascio M (2004) Esquema para interpretação de espectros de substâncias orgânicas na região do infravermelho. Quim Nova 27:670–673

Malavolta E, Vitti GC, Oliveira SA (1997) Evaluation of the nutritional status of plants: principles and applications. Potafos, Piracicaba

Marra R, Vinale F, Cesarano G, Lombardi N, D'Errico G, Crasto A, Mazzei P, Piccolo A, Incerti G, Woo SL, Scala F, Bonanomi G (2018) Biochars from olive mill waste have contrasting effects on plants, fungi and phytoparasitic nematodes. PLoS ONE 13:e0198728. https://doi.org/10.1371/journal.pone.0198728

Mazzei P, Cangemi S, Malakshahi Kurdestani A, Mueller T, Piccolo A (2022) quantitative evaluation of noncovalent interactions between 3,4-dimethyl-1 H-pyrazole and dissolved humic substances by NMR spectroscopy. Environ Sci Technol 56:11771–11779. https://doi.org/10.1021/acs.est.2c00900

Miao W, Li F, Lu J et al (2023) Biochar application enhanced rice biomass production and lodging resistance via promoting co-deposition of silica with hemicellulose and lignin. Sci Total Environ 855:158818

Mukherjee A, Zimmerman AR (2013) Organic carbon and nutrient release from a range of laboratory-produced biochars and biochar-soil mixtures. Geoderma 193–194:122–130

Oguntunde PG, Abiodun BJ, Ajayi AE, Giesen N (2008) Effects of charcoal production on soil physical properties in Ghana. J Plant Nutr Soil Sci 171:591–596

Oukarroum A, Madidi S, Schansker G, Strasser RJ (2007) Probing the responses of barley cultivars (*Hordeum vulgare* L.) by chlorophyll a fluorescence OLKJIP under drought stress and re-watering. Environ Exp Bot 60:438–446. https://doi.org/10.1016/j.envexpbot.2007.01.002

Parfitt RL, Atkinson RJ, Smart SC (1975) The mechanism of phosphate fixation by iron oxides. Soil Sci Soc Amer Proc 39:837–884

Paustian K, Lehmann J, Ogle S, Reay D, Robertson GP, Smith P (2016) Climate-smart soils. Nature 532:49–57

Pospíšil P, Dau H (2000) Chlorophyll fluorescence transients of photosystem II membrane particles as a tool for studying photosynthetic oxygen evolution. Photosyn Res 65:41–52. https://doi.org/10.1023/A:1006469809812

Pradhan S, Abdelaal AH, Mroue K, Al-Ansari T, Mackey HR, McKay G (2020) Biochar from vegetable wastes: agro-environmental characterization. Biochar 2:439–453. https://doi.org/10.1007/s42773-020-00069-9

Preston CM, Nault JR, Trofymow JA (2009) Chemical changes during 6 years of decomposition of 11 litters in some Canadian forest sites. Part 2. 13C abundance, solid-state 13C NMR spectroscopy and the meaning of "lignin." Ecosystems 12:1078–1102. https://doi.org/10.1007/s10021-009-9267-z

Purkaystha J, Prasher S, Afzal MT, Nzediegwu C, Dhiman J (2022) Wheat straw biochar amendment significantly reduces nutrient leaching and increases green pepper yield in a less fertile soil. Environ Technol Innov 28:102655. https://doi.org/10.1016/j.eti.2022.102655

Regmi A, Singh S, Moustaid-Moussa N, Coldren C, Simpson C (2022) The negative effects of high rates of biochar on violas can be counteracted with fertilizer. Plants 11:491. https://doi.org/10.3390/plants11040491

Reza MS, Islam SN, Afroze S, Abu Bakar MS, Sukri RS, Rahman S, Azad AK (2020) Evaluation of the bioenergy potential of invasive *Pennisetum purpureum* through pyrolysis and thermogravimetric analysis. Energy Ecol Environ 5:118–133. https://doi.org/10.1007/s40974-019-00139-0

Robertson SJ, Michael Rutherford P, López-Gutiérrez JC, Massicotte HB (2012) Biochar enhances seedling growth and alters root symbioses and properties of sub-boreal forest soils. Can J Soil Sci 92:329–340. https://doi.org/10.4141/CJSS2011-066

Schmidt HP, Pandit BH, Cornelissen G, Kammann CI (2017) Biochar-based fertilization with liquid nutrient enrichment: 21 field trials covering 13 crop species in Nepal. Land Degrad Dev 28:2324–2342. https://doi.org/10.1002/ldr.2761

Schreiter RIJ, Schmidt W, Kumar A, Graber ER, Schuth C (2020) Effect of water leaching on biochar properties and its impact on organic contaminant sorption. Environ Sci Pollut Res 27:691–703

Semida WM, Beheiry HR, Sétamou M, Simpson CR, Abd El-Mageed TA, Rady MM, Nelson SD (2019) Biochar implications for sustainable agriculture and environment: a review. S Afr J Bot 127:333–347. https://doi.org/10.1016/j.sajb.2019.11.015

Silber A, Levkrovitch I, Graber ER (2010) PH-dependent mineral release and surface properties of cornstraw biochar: agronomic implications. Environ Sci Technol 44:9318–9323

Silva Gonzaga MI, Oliveira da Silva PS, Santos CJ, de Oliveira Junior LFG (2019) Biochar increases plant water use efficiency and biomass production while reducing Cu concentration in Brassica juncea L. in a Cu-contaminated soil. Ecotoxicol Environ Saf 183:109557. https://doi.org/10.1016/j.ecoenv.2019.109557

Souza CCB (2022) Alterações químicas, estruturais e na capacidade de adsorção de metais pesados da cama de frango durante a compostagem. Seropédica, Universidade Federal Rural do Rio de Janeiro, Thesis

Strasser BJ (1997) Donor side capacity of photosystem II probed by chlorophyll a fluorescence transients. Photosyn Res 52:147–155. https://doi.org/10.1023/A:1005896029778

Strasser RJ, Tsimilli-Michael M, Srivastava A (2004) Analysis of the chlorophyll a fluorescence transient. In: Papageorgiou GC and Govindjee (ed) Chlorophyll a fluorescence. Springer, Dordrecht, pp 321–362

Tavares OCH, Santos LA, Filho DF, Ferreira LM, García AC, Castro TAVT, Zonta E, Pereira MG, Fernandes MS (2021) Response surface modeling of humic acid stimulation of the rice (Oryza sativa L.) root system. Arch Agron Soil Sci 67:1046–1059. https://doi.org/10.1080/03650340.2020.1775199

Tomek P, Lazár D, Ilík P, Naus J (2001) On the intermediate steps between the O and P steps in chlorophyll a fluorescence rise measured at different intensities of exciting light. Aust J Plant Physiol 28:1151–1160. https://doi.org/10.1071/pp01065

Torchia DFO, Zonta E, de Andrade AM, García AC (2021) Production and characterization of biochar obtained from different biomass and pyrolysis temperature. Brazilian J Chem Eng 39:415–427. https://doi.org/10.1007/s43153-021-00147-w

Wang L, O'Connor D, Rinklebe J, Ok YS, Tsang DCW, Shen Z, Hou D (2020) Biochar aging: mechanisms, physicochemical changes, assessment, and implications for field applications. Environ Sci Technol 54:14797–14814

Wang W, Zheng J, el Wang Y, al, (2021) Photosynthesis, chlorophyll fluorescence, and yield of peanut in response to biochar application. Front Plant Sci 12:650432

Warnock DD, Lehmann J, Kuyper TW, Rilling MC (2007) Mycorrhizal responses to biochar in soil - concepts and mechanisms. Plant Soil 300:9–20

Wu L, Wei C, Zhang S, Wang Y, Kuzyakov Y, Ding X (2019) MgO-modified biochar increases phosphate retention and rice yields in saline-alkaline soil. J Clean Prod 235:901–909. https://doi.org/10.1016/j.jclepro.2019.07.043

Wu L, Zhang S, Wang J, Ding X (2020) Phosphorus retention using iron (II/III) modified biochar in saline-alkaline soils: adsorption, column and field tests. Environ Pollut 261:114223. https://doi.org/10.1016/j.envpol.2020.114223

Xiao X, Chen Z, Chen B (2016) H/C atomic ratio as a smart linkage between pyrolytic temperatures, aromatic clusters and sorption properties of biochars derived from diverse precursory materials. Sci Rep 6:22644. https://doi.org/10.1038/srep22644

Xu Q, Wang J, Liu Q, Chen Z, Jin P, Du J, Fan J, Yin W, Xie Z, Wang X (2022) Long-term field biochar application for rice production: effects on soil nutrient supply, carbon sequestration, crop yield and grain minerals. Agronomy 12:1924. https://doi.org/10.3390/agronomy12081924

Yin Q, Wang R, Zhao Z (2018) Application of Mg–Al-modified biochar for simultaneous removal of ammonium, nitrate, and phosphate from eutrophic water. J Clean Prod 176:230–240. https://doi.org/10.1016/j.jclepro.2017.12.117

Yusuf MA, Kumar D, Rajwanshi R, Strasser RJ, Tsimilli-Michael M, Govindjee Sarin NB (2010) Overexpression of γ-tocopherol methyl transferase gene in transgenic Brassica juncea plants alleviates abiotic stress: physiological and chlorophyll a fluorescence measurements. Biochim Biophys Acta Bioenerg 1797:1428–1438. https://doi.org/10.1016/j.bbabio.2010.02.002

Zhang ZS, Song XL, Lu XG, Xue ZS (2013) Ecological stoichiometry of carbon, nitrogen, and phosphorus in estuarine wetland soils: influences of vegetation coverage, plant communities, geomorphology, and seawalls. J Soils Sediments 13:1043–1051. https://doi.org/10.1007/s11368-013-0693-3

Authors and Affiliations

Danielle França de Oliveira Torchia[1] [ORCID] **· Tadeu Augusto van Tol de Castro[1] · Orlando Carlos Huertas Tavares[1] · Camila Costa Barros Souza[2] · Hellen Fernanda Oliveira da Silva[1] · Octávio Vioratti Telles de Moura[1] · Kimberly Christina Marques da Silva[1] · Franciele de Souza Rocha[1] · Everaldo Zonta[3] · Andrés Calderín García[1]**

✉ Danielle França de Oliveira Torchia
dani.foliveira@hotmail.com

[1] Laboratory of Soil Biological Chemistry, Department of Soils, Federal Rural University of Rio de Janeiro, Seropédica, RJ, Brazil

[2] Laboratory of Soil Chemistry, Department of Soils, Federal Rural University of Rio de Janeiro, Seropédica, RJ, Brazil

[3] Laboratory of Soil and Plant, Department of Soils, Federal Rural University of Rio de Janeiro, Seropédica, RJ, Brazil